



Aalborg Universitet

AALBORG UNIVERSITY
DENMARK

Coordinated control to achieve stability and dynamic response enhancement of weak-grid-connected inverters based on sequence-admittance models

Yu, Yanxue; Zheng, Xuemei; Li, Haoyu; Guerrero, Josep M.; Akhavan, Ali

Published in:
IET Renewable Power Generation

DOI (link to publication from Publisher):
[10.1049/rpg2.12327](https://doi.org/10.1049/rpg2.12327)

Creative Commons License
CC BY 4.0

Publication date:
2022

Document Version
Publisher's PDF, also known as Version of record

[Link to publication from Aalborg University](#)

Citation for published version (APA):
Yu, Y., Zheng, X., Li, H., Guerrero, J. M., & Akhavan, A. (2022). Coordinated control to achieve stability and dynamic response enhancement of weak-grid-connected inverters based on sequence-admittance models. *IET Renewable Power Generation*, 16(2), 339-351. <https://doi.org/10.1049/rpg2.12327>

General rights


Copyright and moral rights for the publications made accessible in the public portal are retained by the authors and/or other copyright owners and it is a condition of accessing publications that users recognise and abide by the legal requirements associated with these rights.

- Users may download and print one copy of any publication from the public portal for the purpose of private study or research.
- You may not further distribute the material or use it for any profit-making activity or commercial gain
- You may freely distribute the URL identifying the publication in the public portal -

Take down policy

If you believe that this document breaches copyright please contact us at vbn@aub.aau.dk providing details, and we will remove access to the work immediately and investigate your claim.

Coordinated control to achieve stability and dynamic response enhancement of weak-grid-connected inverters based on sequence-admittance models

Yanxue Yu¹ | Xuemei Zheng¹  | Haoyu Li¹ | Josep M. Guerrero² | Ali Akhavan²

¹ School of Electrical Engineering and Automation, Harbin Institute of Technology, Harbin, China

² Department of Energy Technology, Aalborg University, Aalborg, Denmark

Correspondence

Xuemei Zheng, School of Electrical Engineering and Automation, Harbin Institute of Technology, Harbin, China.

Email: xmzheng@hit.edu.cn

Funding information

National Natural Science Foundation of China, Grant/Award Number: 62073095; State Grid Heilongjiang Electric Power Co., Ltd, Grant/Award Number: 522437200038

Abstract

In grid-connected inverters (GCIs), the phase-locked loop (PLL) behaves as a negative admittance at the point of common coupling (PCC), composed of both the PLL controller and current controller terms. Therefore, not only the PLL dynamics, but also dynamical interactions between the PLL controller and current controller might trigger instabilities in weak grids, which complicates the controller parameters regulation. The smaller PLL bandwidth could help to mitigate the instabilities, but at the expense of sacrificing the system dynamic response. In view of this, a coordinated control composed of the q -axis voltage and PCC-voltage feedforward based on sequence-admittance models is proposed here. The q -axis voltage feedforward is designed with a simple proportional feedforward coefficient to make the PLL-induced negative admittance insensitive to the PLL controller parameters. In other words, the PLL bandwidth would not be limited by the stability requirements and the dynamic response speed could be ensured. Furthermore, the PCC-voltage feedforward is developed to coordinate the q -axis voltage feedforward by phase compensation, thus to achieve stability improvement. Finally, simulations and hardware-in-the-loop tests are carried out to verify the enhanced stability and dynamic response of the modified GCI with the proposed coordinated control in weak grid.

1 | INTRODUCTION

The phase-locked loop (PLL) is a commonly used unit of grid-connected inverters (GCIs) to achieve synchronization with the power grid [1–4]. Ideally, the PLL should be designed to extract the amplitude and phase of the grid voltage, regardless of grid conditions and behaviours of the GCIs [1]. While, in weak grid, the large grid impedance would affect the performance of the PLL [2] and cause interactions between the PLL and current control [3, 4]. According to the existing researches, the interactions are easier to trigger instabilities of GCIs ranging from several Hz to several hundred Hz [5, 6]. Reducing the PLL bandwidth would contribute to mitigate the instabilities of GCIs in weak grid, but at the expense of sacrificing the system dynamic response. Therefore, it is required to attenuate the PLL-related instabilities considering

the dynamic response performance simultaneously in weak grid.

The impedance or admittance models are widely developed to characterize and analyse the PLL-related instabilities [7–14]. It has been pointed out the PLL can be modelled as a paralleled impedance at the point of common coupling (PCC) that shows negative resistance property within its control bandwidth [8, 9, 11], which would result in low-frequency resonances. Based on the developed impedance models, common recognitions towards the PLL can be concluded that: (1) The weak grid and the large penetration level of the power generating units could strengthen the PLL's negative dynamic effect [2]; (2) Decreasing the PLL bandwidth contributes to attenuate the negative resistance, but it sacrifices the system dynamical performance [11]; (3) If not designed properly, the PLL controller could further interact with the current controller because of the control band

This is an open access article under the terms of the [Creative Commons Attribution](https://creativecommons.org/licenses/by/4.0/) License, which permits use, distribution and reproduction in any medium, provided the original work is properly cited.

© 2021 The Authors. *IET Renewable Power Generation* published by John Wiley & Sons Ltd on behalf of The Institution of Engineering and Technology

overlap effect, which could result in harmonic resonance [3, 4, 15, 16]; (4) The asymmetrical structure of the PLL could result in frequency-couplings, so sub- and near-synchronous oscillations might be triggered together, which can propagate in the power system [12–14]. In view of the above problems, some stability improvement methods towards the PLL have also been proposed.

Representatively, considering the interactions between the PLL controller and current controller, an improved design of the current controller and an improved design of the PLL controller were proposed in [3] and [4], based on the q -axis impedance, respectively. That reduces the negative effect of PLL on current control and enhances the stability in weak grids, but the controller parameters are confined by the stability regions that need to be redrawn towards different GCIs. Based on the online grid impedance estimation, [11] proposed a PLL bandwidth adaptive control method to retain the dynamic performance maximumly based on sequence-impedances to cope with the variation of grid impedance. Besides the controller offline or online regulation methods, additional feedforward or feedback control loops were also designed to attenuate the negative effect of the PLL. Accordingly, [9] developed an impedance controller based on the q -axis voltage feedforward for turning the q -axis impedance into a positive resistance in the low-frequency band. Zhang et al. [17] modified the grid voltage feedforward control to compensate for the PLL perturbations and revised the dq -domain output impedance. Chen et al. [18] come up with a novel impedance-phased compensation control strategy to increase the system phase margin. Recently, some symmetrical control methods were proposed to address the frequency-coupling problem. In [19], a symmetrical PLL was designed according to the concept of complex phase angle vector. It eliminates the frequency-coupling terms, but the PLL bandwidth is still limited by the weak grid. In [20], a q -axis feedforward and d -axis compensation control methods were proposed to decrease the asymmetric influence caused by the PLL. Moreover, [21] designed a voltage-modulated direct power control, which removed the PLL, totally. However, without extra filters, the PLL-eliminate methods are not applicable to the weak and distorted grids [22].

To sum up, it is difficult to achieve decoupling design of the PLL controller and current controller and suppress the PLL-induced resonances without sacrificing system dynamic response. Most existing works develop the improvement methods based on the dq -domain impedances and take the stability as a prerequisite to reshape the output impedance. Additionally, the existing feedforward methods aiming at maximumly compensating the PLL-induced negative resistance are usually designed with complex coefficients. Although some control schemes are proposed with the PLL-less structures, it is not easy for them to adapt to complex grid environments. In order to solve the above-mentioned issues resulting from the PLL, considering the advantages of sequence-impedance models, this paper proposes a coordinated control method composed of a q -axis voltage and PCC-voltage feedforward control loop to reshape the sequence-admittances. The former modifies the sequence-admittances insensitive to the PLL controller param-

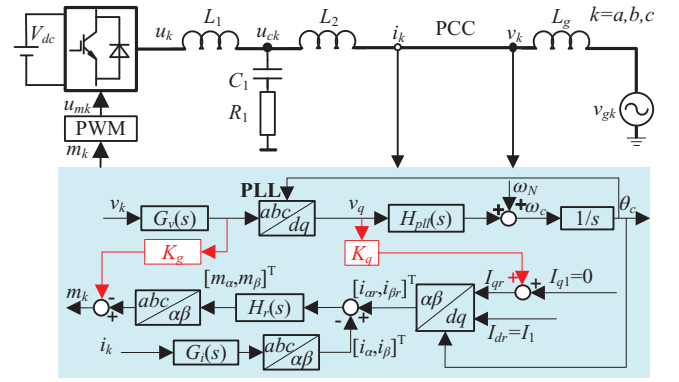


FIGURE 1 Topology and control scheme of the GCI with the proposed coordinated control

eters and gains decoupling design between the PLL and current controller, thus the PLL design procedure is independent and its dynamic response can be enhanced; the latter is developed to compensate for the phase lag of the GCI with the designed q -axis voltage feedforward, thus ensures the overall stability of the modified GCI in weak grids.

This paper is organized as follows. Section 2 introduces the modified GCI with the proposed coordinated control and corresponding sequence-domain admittance models are built. Section 3 designs feedforward coefficients of the coordinated control to reshape sequence-admittances of the GCI according to the stability and dynamic performance. Furthermore, Section 4 reveals the stability of the modified GCI in weak grid by comparison with that of the traditional GCI based on the developed sequence-admittance models. Section 5 carries out simulations based on the *Plecs* and RT-Box to validate the effectiveness of the proposed coordinated control method. Section 6 concludes the paper.

2 | MODELLING OF THE MODIFIED GCI WITH THE PROPOSED COORDINATED CONTROL

2.1 | Structure of the modified GCI with the proposed coordinated control

Figure 1 shows the topology and control scheme of the modified GCI with the proposed coordinated control, composed of a q -axis voltage and PCC-voltage feedforward control loop, where K_q is the q -axis voltage feedforward coefficient and K_g is the PCC-voltage feedforward coefficient.

In Figure 1, V_{dc} is the dc-side voltage; u_k , u_{ck} , v_k and v_{gk} ($k = a, b, c$) represent the output voltage of the three-phase bridge, voltage across the capacitance branch, voltage at the PCC, and the grid voltage, respectively. i_k is the grid-connected current and also the controlled current. R_1 is the damping resistance added to the L_1 - C_1 - L_2 filter; L_g represents the grid inductance. The GCI is controlled in $\alpha\beta$ -domain and the classical synchronous-reference-frame controlled PLL is the studied

object. In the control loop, $G_v(s)$ and $G_i(s)$ describe the voltage and current sampling transfer functions, respectively; I_1 and I_{q1} denote the given active and reactive power current, where I_{q1} is set to zero to ensure the unit power factor; I_{dr} and I_{qr} are the dq -axis current references; $i_{\alpha r}$ and $i_{\beta r}$ are the $\alpha\beta$ -axis current references generated from I_{dr} and I_{qr} by dq -to- $\alpha\beta$ transformation with the PLL locked phase θ_c ; i_α and i_β are the sampled $\alpha\beta$ -axis currents; $H_r(s)$ denotes the proportional resonant (PR) current controller that is presented as Equation (1), where K_{pr} and K_{rr} are the proportional and resonant coefficient, respectively; m_k represents the PWM modulation wave; u_{mk} is the switch signal.

$$H_r(s) = K_{pr} + \frac{K_{rr}s}{s^2 + \omega_1^2} \quad (1)$$

In the PLL control loop, only the q -axis voltage is used to derive the synchronization phase θ_c , which expresses the asymmetrical feature of the PLL. ω_N is the given angular frequency; ω_c is the output angular frequency; $H_{pll}(s)$ is the proportional-integral (PI) controller for the PLL that is presented as Equation (2), where K_p and K_i denote the proportional and integral coefficients, respectively. With the introduced q -axis voltage feedforward control, it can be seen that dynamics of the q -axis voltage are introduced to I_{qr} .

$$H_{pll}(s) = K_p + \frac{K_i}{s} \quad (2)$$

2.2 | Sequence-admittance modelling of the modified GCI

According to the harmonic linearization method [11], it is required to superimpose a small voltage perturbation on the fundamental voltage at PCC. Taking phase A as an example, the perturbed voltage v_a can be written as:

$$v_a(t) = V_1 \cos(2\pi f_1 t) + V_p \cos(2\pi f_p t + \varphi_{vp}) + V_n \cos(2\pi f_n t + \varphi_{vn}) \quad (3)$$

where V_1 and f_1 are the amplitude and frequency of the fundamental voltage; V_p, f_p , and φ_{vp} are the amplitude, frequency, and phase of the positive-sequence voltage perturbation; V_n, f_n , and φ_{vn} are the amplitude, frequency, and phase of the negative-sequence voltage perturbation. By rewriting Equation (3) in frequency-domain, v_a can be written as:

$$V_a[f] = \begin{cases} \mathbf{V}_1 = V_1/2, & f = \pm f_1 \\ \mathbf{V}_p = (V_p/2)e^{\pm j\varphi_{vp}}, & f = \pm f_p \\ \mathbf{V}_n = (V_n/2)e^{\pm j\varphi_{vn}}, & f = \pm f_n \end{cases} \quad (4)$$

where the bold capital letters represent the frequency-domain descriptions, including the amplitude and the phase information of the signal at certain frequencies. The perturbed voltage v_b and v_c can be described similarly.

For the PLL, the PCC voltage under perturbation is sampled for synchronization. Thus, the output phase θ_c is not equal to the fundamental voltage phase $\theta_1 = 2\pi f_1 t$, it contains the small-signal response $\Delta\theta$, which can be derived as [11]:

$$\Delta\theta[f] = \begin{cases} \mp j F_{pll}(s) \mathbf{V}_p G_v(s \pm j\omega_1), & f = \pm(f_p - f_1) \\ \pm j F_{pll}(s) \mathbf{V}_n G_v(s \mp j\omega_1), & f = \pm(f_n + f_1) \end{cases} \quad (5)$$

where $F_{pll}(s) = [H_{pll}(s)/s]/[1 + V_1 H_{pll}(s)/s]$, $\omega_1 = 2\pi f_1$.

Considering that $\cos\theta_c[f] \approx \cos\theta_1[f] - \Delta\theta[f] * \sin\theta_1[f]$, where $*$ denotes the convolution operation, it can be obtained that:

$$\cos\theta_c[f] = \begin{cases} 0.5, & f = \pm f_1 \\ 0.5 F_{pll}(s \mp j\omega_1) G_v(s) \mathbf{V}_p, & f = \pm f_p \\ -0.5 F_{pll}(s \pm j\omega_1) G_v(s \pm j2\omega_1) \mathbf{V}_p, & f = \pm(f_p - 2f_1) \\ 0.5 F_{pll}(s \pm j\omega_1) G_v(s) \mathbf{V}_n, & f = \pm f_n \\ -0.5 F_{pll}(s \mp j\omega_1) G_v(s \mp j2\omega_1) \mathbf{V}_n, & f = \pm(f_n + 2f_1) \end{cases} \quad (6)$$

Additionally, $\sin\theta_c[f] = \mp j \cos\theta_c[f]$. Substituting $\cos\theta_c[f]$ and $\sin\theta_c[f]$ to the abc -to- dq transformation, the following equation for v_q in the frequency-domain could be obtained.

$$V_q[f] = \begin{cases} 0, & dc \\ \mp j G_v(s \pm j\omega_1) \mathbf{V}_p [1 - V_1 F_{pll}(s)], & f = \pm(f_p - f_1) \\ \pm j G_v(s \mp j\omega_1) \mathbf{V}_n [1 - V_1 F_{pll}(s)], & f = \pm(f_n + f_1) \end{cases} \quad (7)$$

Then, the q -axis current reference I_{qr} is modified as $I_{qr}[f] = V_q[f] K_q$. According to the dq -to- $\alpha\beta$ transformation with θ_c , the α -axis current reference $i_{\alpha r}$ can be calculated from $I_{\alpha r}[f] = I_1 * \cos\theta_c[f] - I_{qr} * \sin\theta_c[f]$, which is written as Equation (8). It can be seen that the disturbed voltage results in current response not only at corresponding frequency f_p and f_n , but also at coupled frequency $(f_p - 2f_1)$ and $(f_n + 2f_1)$. That is the

frequency-coupling phenomena.

$$I_{\alpha r}[f] = \begin{cases} 0.5I_1, f = \pm f_1 \\ 0.5 [(I_1 - V_1K_q)F_{pLL}(s \mp j\omega_1) + K_q] \cdot \\ G_v(s)\mathbf{V}_p, f = \pm f_p \\ 0.5 [(V_1K_q - I_1)F_{pLL}(s \pm j\omega_1) - K_q] \cdot \\ G_v(s \pm j2\omega_1)\mathbf{V}_p, f = \pm(f_p - 2f_1) \\ 0.5 [(I_1 - V_1K_q)F_{pLL}(s \pm j\omega_1) + K_q] \cdot \\ G_v(s)\mathbf{V}_n, f = \pm f_n \\ 0.5 [(V_1K_q - I_1)F_{pLL}(s \mp j\omega_1) - K_q] \\ G_v(s \mp j2\omega_1)\mathbf{V}_n, f = \pm(f_n + 2f_1) \end{cases} \quad (8)$$

Supposing the frequency-domain current response of phase A at PCC is described as Equation (9), where I_1 and φ_{i1} are the amplitude and phase of the fundamental current response; I_p and φ_{ip} are the amplitude and phase of the current response at the perturbed positive-sequence frequency f_p ; I_n and φ_{in} are the amplitude and phase of the current response at the perturbed negative-sequence frequency f_n ; I_{np} and φ_{inp} are the amplitude and phase of the current response at the coupled negative-sequence frequency ($f_p - 2f_1$); I_{pn} and φ_{ipn} are the amplitude and phase of the current response at the coupled positive-sequence frequency ($f_n + 2f_1$). After the abc -to- $\alpha\beta$ transformation, $I_{\alpha}[f] = I_a[f]$.

$$I_a[f] = \begin{cases} \mathbf{I}_1 = (I_1/2)e^{\pm j\varphi_{i1}}, f = \pm f_1 \\ \mathbf{I}_p = (I_p/2)e^{\pm j\varphi_{ip}}, f = \pm f_p \\ \mathbf{I}_{np} = (I_{np}/2)e^{\pm j\varphi_{inp}}, f = \pm(f_p - 2f_1) \\ \mathbf{I}_n = (I_n/2)e^{\pm j\varphi_{in}}, f = \pm f_n \\ \mathbf{I}_{pn} = (I_{pn}/2)e^{\pm j\varphi_{ipn}}, f = \pm(f_n + 2f_1) \end{cases} \quad (9)$$

According to the current control scheme as depicted in Figure 1, it can be acquired that:

$$\langle \{I_{\alpha r}[f] - I_{\alpha}[f]\} \cdot H_r(s) - K_g G_v(s)v_k(s) \rangle G_d(s) = u_k(s) \quad (10)$$

where $G_d(s) = e^{-1.5sT_s}$ represents the time delay. T_s is the sampling period.

From the main circuit of the GCI in Figure 1, the relationship among u_k , v_k and i_k in frequency-domain can be deduced as:

$$u_k(s) = \left[L_1 L_2 s^2 \cdot \frac{1}{R_1 + 1/(sC_1)} + (L_1 + L_2)s \right] \cdot i_k(s) + \left[L_1 s \cdot \frac{1}{R_1 + 1/(sC_1)} + 1 \right] \cdot v_k(s) \quad (11)$$

For simplicity, $P_1(s) = L_1 L_2 s^2 / [R_1 + 1/(sC_1)] + s(L_1 + L_2)$ and $P_2(s) = L_1 s / [R_1 + 1/(sC_1)] + 1$ are defined as the LCL-related coefficients.

By substituting Equations (8), (9), and (11) into Equation (10), sequence-admittances of the modified GCI with the coordinated control can be obtained as follows:

$$Y_{\varphi p}(s) = -\frac{\mathbf{I}_p}{\mathbf{V}_p} = \frac{P_2(s) + K_g G_v(s)G_d(s) + G_v(s)G_d(s)H_r(s) \cdot [0.5(V_1K_q - I_1)F_{pLL}(s \mp j\omega_1) - 0.5K_q]}{G_d(s)H_r(s)G_i(s) + P_1(s)}, \quad f = \pm f_p \quad (12)$$

$$J_{\varphi p}(s) = -\frac{\mathbf{I}_{np}}{\mathbf{V}_p} = \frac{G_v(s \pm j2\omega_1)H_r(s)G_d(s) \cdot [0.5(I_1 - V_1K_q)F_{pLL}(s \pm j\omega_1) + 0.5K_q]}{G_d(s)H_r(s)G_i(s) + P_1(s)}, \quad f = \pm(f_p - 2f_1) \quad (13)$$

$$Y_{\varphi n}(s) = -\frac{\mathbf{I}_n}{\mathbf{V}_n} = \frac{P_2(s) + K_g G_v(s)G_d(s) + G_v(s)G_d(s)H_r(s) \cdot [0.5(V_1K_q - I_1)F_{pLL}(s \pm j\omega_1) - 0.5K_q]}{G_d(s)H_r(s)G_i(s) + P_1(s)}, \quad f = \pm f_n \quad (14)$$

$$J_{\varphi n}(s) = -\frac{\mathbf{I}_{pn}}{\mathbf{V}_n} = \frac{G_v(s \mp j2\omega_1)H_r(s)G_d(s) \cdot [0.5(I_1 - V_1K_q)F_{pLL}(s \mp j\omega_1) + 0.5K_q]}{G_d(s)H_r(s)G_i(s) + P_1(s)}, \quad f = \pm(f_n + 2f_1) \quad (15)$$

where $Y_{\varphi p}(s)$ and $Y_{\varphi n}(s)$ are the positive-sequence and negative-sequence self-admittances (SAs) of the modified GCI, respectively; $J_{\varphi p}(s)$ and $J_{\varphi n}(s)$ are the coupled-admittances (CAs) of the modified GCI resulting from positive-sequence and negative-sequence voltage perturbations, respectively.

As for the traditional GCI, namely $K_q = K_g = 0$, corresponding SA and CA under the positive-sequence voltage perturbation can be written as:

$$Y_p(s) = \frac{P_2(s) - G_v(s)G_d(s)H_r(s) \cdot 0.5I_1 F_{pLL}(s \mp j\omega_1)}{G_d(s)H_r(s)G_i(s) + P_1(s)}, \quad f = \pm f_p \quad (16)$$

$$J_p(s) = \frac{G_v(s \pm j2\omega_1)G_d(s)H_r(s) \cdot 0.5I_1 F_{pLL}(s \pm j\omega_1)}{G_d(s)H_r(s)G_i(s) + P_1(s)}, \quad f = \pm(f_p - 2f_1) \quad (17)$$

If the PLL dynamics are neglected, $Y_p(s)$ and $J_p(s)$ would be simplified as $Y_p(s) = P_2(s)/[G_d(s)H_r(s)G_i(s)+P_1(s)]$ and $J_p(s) = 0$. That indicates the PLL introduces not only a negative admittance term, but also the frequency-coupling term, which could result in resonances. Additionally, it should be mentioned that the added negative admittance contains dynamical interactions between the PLL controller and current controller, which would deteriorate the PLL-induced resonances.

While, if the coordinated control is introduced, the influences of the PLL dynamics via $F_{pll}(s)$ could be modified by the q -axis voltage feedforward coefficient K_q , and the overall frequency characteristics of SAs could be adjusted by the PCC-voltage feedforward coefficient K_g .

3 | FEEDFORWARD COEFFICIENTS DESIGN OF THE COORDINATED CONTROL

The above analyses show that control dynamics of the PLL need to be fully considered. According to previous researches, the higher PLL bandwidth would increase the interactions between the PLL control and current control and result in more severe resonances. While, the lower PLL bandwidth would influence the dynamic response speed. To balance the stability and dynamic performance of the GCI, feedforward coefficients of the coordinated control are designed as follows.

3.1 | Design of the q -axis voltage feedforward coefficient K_q

Firstly, the q -axis voltage feedforward coefficient K_q is designed. From Equation (12) to Equation (15), it can be clearly seen that if K_q is chosen to be I_1/V_1 , the coefficients of $F_{pll}(s \pm j\omega_1)$ and $F_{pll}(s \mp j\omega_1)$ would be zero, which means that the modified sequence-admittances have no relationships with the PLL control dynamics. The PLL controller can be designed independently with satisfied dynamical performance. Additionally, the coupling terms between the PLL controller and current controller are removed from sequence-admittance models.

If only the q -axis voltage feedforward with $K_q = I_1/V_1$ is added to the GCI, with the system parameters shown in Table 1, the Bode-plotted sequence admittances and corresponding measurement results are shown in Figure 2. Where, the PLL controller parameters are designed according to the typical second-order system [15], whose bandwidth and damping ratio is 200 Hz and 0.707, respectively.

In Figure 2, the measured dots are consistent with corresponding solid lines, which validates the correctness of the built sequence-admittance models. Additionally, sequence-admittances of the GCI without the q -axis voltage feedforward ($K_q = 0$) are depicted as dotted lines to recognize the frequency characteristics of the modified sequence-admittances better. By comparison, it could be concluded that: (1) For the magnitude-frequency plots, the major difference of sequence-admittances between $K_q = I_1/V_1$ and $K_q = 0$ locates at the frequencies which

TABLE 1 Main system parameters of the studied GCI

Parameters	Value	Parameters	Value
L_1	2.2 mH	L_2	2.2 mH
C_1	10 μ F	R_1	3.5 Ω
V_{dc}	700 V	V_1	311 V
f_i	10 kHz	T_s	1×10^{-4} s
f_1	50 Hz	$H_r: (K_{pr}, K_{rr})$	(15, 15,000)
I_1/I_{q1}	20 A/0 A	$H_{pll}: (K_p, K_i)$	(2.775, 1198)
ω_N	314 rad/s	K_q	0.0643

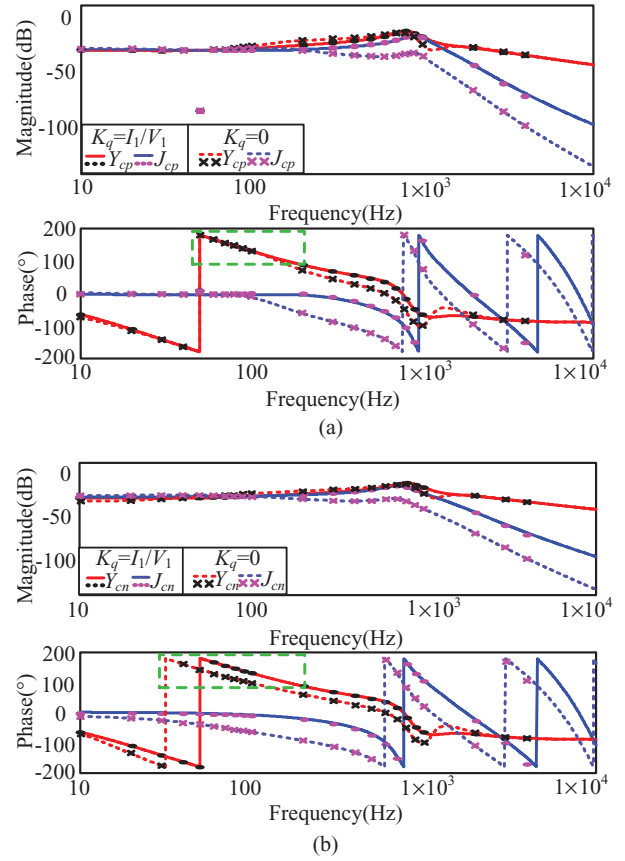


FIGURE 2 Sequence-admittances validation and comparison of the modified GCI with different K_q . (a) Sequence-admittances under the positive-sequence perturbation, (b) sequence-admittances under the negative-sequence perturbation

are above 200 Hz, especially for the CAs. Additionally, magnitudes of SAs and CAs with $K_q = I_1/V_1$ are close to each other within 1000 Hz, while magnitudes of SAs and CAs with $K_q = 0$ only show closeness within 200 Hz. That indicates the added q -axis voltage feedforward would exaggerate the frequency-coupling phenomenon in a wider frequency range. (2) For the phase-frequency plots, the phase of SAs with $K_q = I_1/V_1$ is higher than that of SAs with $K_q = 0$ from 50 to 1000 Hz. That indicates the negative damping regions are enlarged by setting $K_q = I_1/V_1$ as circled by green rectangles.

Therefore, the designed q -axis voltage feedforward with $K_q = I_1/V_1$ eliminates the stability requirements for the PLL bandwidth and the PLL dynamic response speed could be ensured, but the PLL-induced resonance might be worse with the enlarged frequency-coupling and negative damping characteristics. That is because the PLL still introduces a negative admittance term written as Equation (18) when $K_q = I_1/V_1$. It is known for the traditional GCI that the negative admittance is shown as Equation (19). The $F_{pll}(s)$ in Equation (19) can be simplified as $1/V_1$ within its control bandwidth. That is to say, if the PLL bandwidth is large enough, Equation (19) would be equal to Equation (18), which indicates the decreased stability of the GCI with the designed q -axis voltage feedforward coefficient.

$$Y_{pll}^1(s) = \frac{-0.5(I_1/V_1)G_v(s)H_r(s)G_d(s)}{G_d(s)H_r(s)G_i(s) + P_1(s)}, f = \pm f_p \quad (18)$$

$$Y_{pll}^2(s) = \frac{-0.5I_1F_{PLL}(s \mp j\omega_1)G_v(s)H_r(s)G_d(s)}{G_d(s)H_r(s)G_i(s) + P_1(s)}, f = \pm f_p \quad (19)$$

Additionally, it should be mentioned that the designed q -axis voltage feedforward would change with I_1 or/and V_1 varying. As the stability of the PLL-CCI is closely connected with I_1 [2, 11], the term I_1 in $K_q = I_1/V_1$ keeps consistent with the value of the active current that given directly or calculated from the generated active power. Considering the fluctuation of the grid voltage amplitude V_1 is mostly controlled within 10%, the term V_1 in $K_q = I_1/V_1$ is set to the rated grid voltage. Influences of the grid voltage fluctuation would be given in the following stability analyses.

With the same control scheme, in [9], the q -axis voltage feedforward control is designed with a negative feedforward coefficient, which is written as $K_q(z) = -F_{pll}(z)[V_1/H_r(z) + I_1]$ to cancel out the PLL-induced negative impedance term of the q -axis impedance completely. Comparatively, the q -axis voltage feedforward control utilized in this paper is designed via sequence-admittance models to just eliminate the influence of the PLL controller parameters with a much simpler feedforward coefficient.

3.2 | Design of the PCC-voltage feedforward coefficient K_g

In order to preserve the advantages of the modified GCI with $K_q = I_1/V_1$ and attenuate the decreased stability, the PCC-voltage feedforward depicted in Figure 1 is introduced. The PCC-voltage feedforward coefficient K_g is chosen as a low-pass filter to achieve phase-compensation without sacrificing the enhanced dynamic response of the GCI with $K_q = I_1/V_1$, which is written as:

$$K_g = \frac{1}{s/(2\pi f_L) + 1} \quad (20)$$

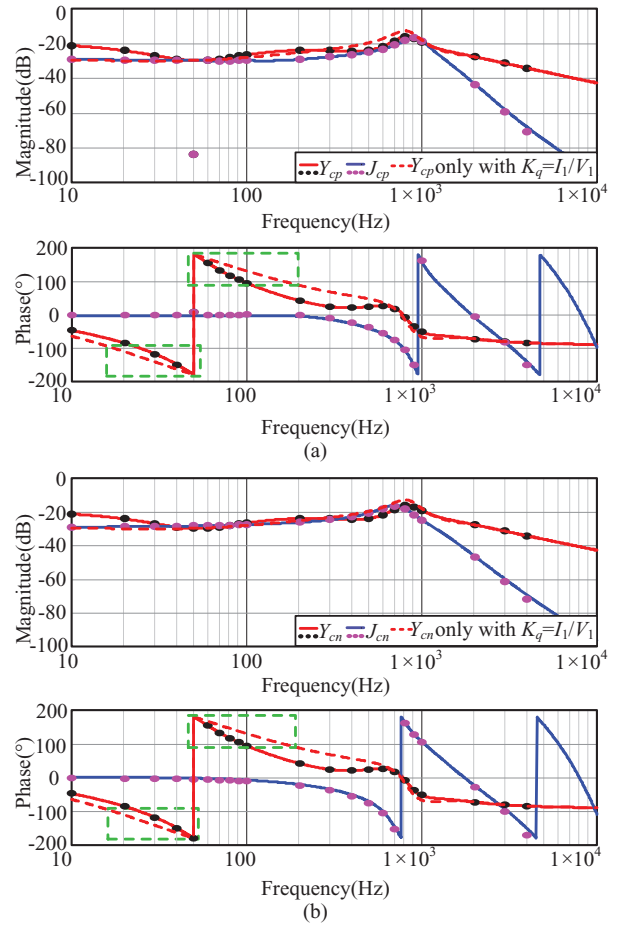


FIGURE 3 Sequence-admittances validation and comparison of the modified GCI with the proposed coordinated control. (a) Sequence-admittances under the positive-sequence perturbation, (b) Sequence-admittances under the negative-sequence perturbation

where f_L denotes the cut-off frequency of the low-pass filter.

With the parameters in Table 1, Figure 3 shows the built sequence-admittances and their measurement results of the GCI with the designed PCC-voltage feedforward control coordinating the q -axis voltage feedforward control, where $f_L = 200$ Hz. From Figure 3, it can be seen the measured points validate the solid-line-represented sequence-admittance models well. Additionally, $Y_{\varphi}(s)$ and $Y_{cn}(s)$ only with $K_q = I_1/V_1$ is depicted as red dotted lines for comparison. It can be clearly seen that the phase of $Y_{\varphi}(s)$ and $Y_{cn}(s)$ with the coordinated control are much smaller than that of $Y_{\varphi}(s)$ and $Y_{cn}(s)$ with only $K_q = I_1/V_1$, which verifies the phase-compensation effect of the added PCC-voltage feedforward. Therefore, the designed K_g suppresses the PLL-related negative damping effectively.

In Figure 3, the cut-off frequency f_L is 200 Hz. If the f_L is designed to be other values, corresponding frequency-characteristics of $Y_{\varphi}(s)$ are shown in Figure 4. With f_L increased from 100 to 300 Hz, the phase of $Y_{\varphi}(s)$ is almost the same and it can be observed the magnitude of $Y_{\varphi}(s)$ becomes larger between 100 and 500 Hz and becomes smaller between 500 and 1000 Hz. As the coupled admittance $J_{\varphi}(s)$ is not influenced by the PCC-voltage feedforward, the coupling of $Y_{\varphi}(s)$ and $J_{\varphi}(s)$

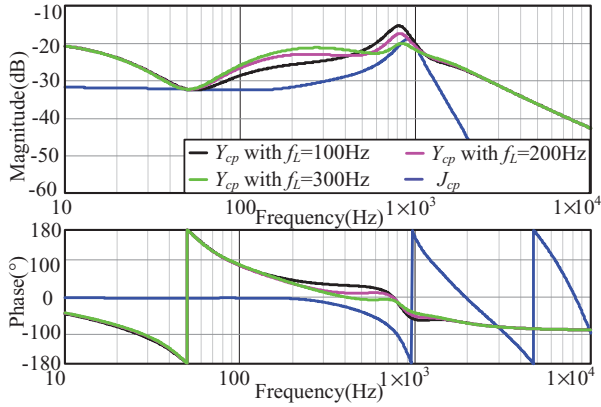


FIGURE 4 Corresponding comparison of sequence-admittances of the modified GCI with different f_L

would be weaker between 100 and 500 Hz and stronger between 500 and 1000 Hz with the larger f_L . Considering that the coupling of $Y_{cp}(s)$ and $J_{cp}(s)$ would deteriorate the stability, the f_L cannot be too large or too small to ensure a better stability condition in a wide frequency range, which is chosen to be 200 Hz to make a compromise.

The PCC-voltage feedforward has been widely applied in GCIs to increase the dynamical performances, attenuate the grid harmonics, suppress the inrush current, and even improve the interactive stability [9]. The application in this paper mainly aims at cooperating with the designed q -axis voltage feedforward to ensure the stability and dynamic response performance of the GCIs. Moreover, the designed coefficients are much easier to be implemented.

4 | STABILITY ANALYSIS OF THE MODIFIED GCI WITH THE PROPOSED COORDINATED CONTROL

Because of the frequency-coupling phenomenon, according to [22], the equivalent sequence-admittance models should be applied to analyse the coupling-related interactive stability between the GCI and the grid, which are written as follows:

$$Y_{ep}(s) = Y_{cp}(s) - \frac{J_{cp}(s)J_{cn}(s \mp j2\omega_1)Z_{gn}(s \mp j2\omega_1)}{1 + Y_{cn}(s \mp j2\omega_1)Z_{gn}(s \mp j2\omega_1)} \quad (21)$$

$$Y_{en}(s) = Y_{cn}(s) - \frac{J_{cn}(s)J_{cp}(s \pm j2\omega_1)Z_{gp}(s \pm j2\omega_1)}{1 + Y_{cp}(s \pm j2\omega_1)Z_{gp}(s \pm j2\omega_1)} \quad (22)$$

where $Y_{ep}(s)$ and $Y_{en}(s)$ are the equivalent positive-sequence and negative-sequence admittances, respectively; $Z_{gp}(s)$ and $Z_{gn}(s)$ are the positive-sequence and negative-sequence impedances of the grid, respectively.

With the developed equivalent sequence-admittance models, stability conclusions can be drawn by analysis of the SISO models $Y_{ep}(s)Z_{gp}(s)$ and $Y_{en}(s)Z_{gn}(s)$, if they don't encircle the

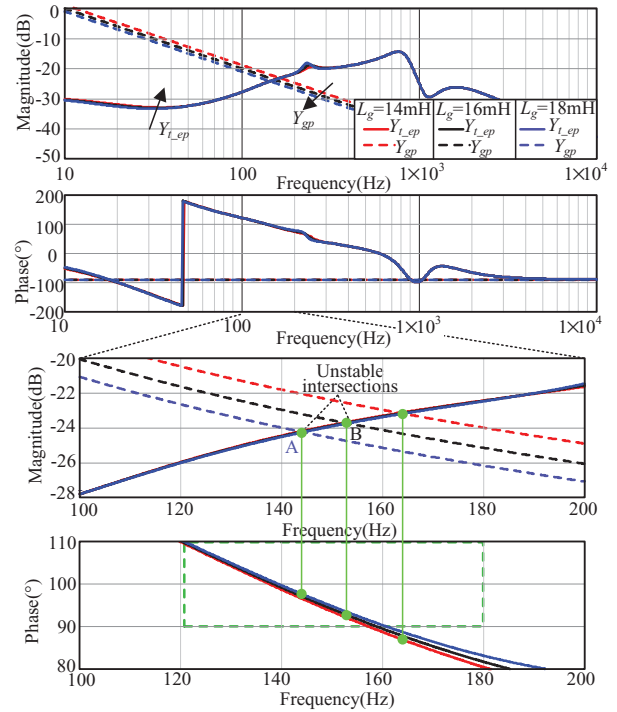


FIGURE 5 Admittances of the grid and the traditional GCI under different L_g

point $(-1, j0)$, stability of the GCI could be satisfied [7]. Taking the positive-sequence as an example, corresponding unstable conclusions could be derived based on Bode plots if: (1) The magnitude-frequency plot of $Y_{ep}(s)$ and that of $Y_{gp}(s)$ have intersections, where $Y_{gp}(s) = 1/Z_{gp}(s)$; (2) the phase difference between $Y_{ep}(s)$ and $Y_{gp}(s)$ at the intersection exceeds 180° . In this paper, we will analyse the system stability through the positive-sequence stability analysis model $Y_{ep}(s)/Y_{gp}(s)$ [11].

4.1 | Stability analysis of the traditional GCI

When $K_q = K_g = 0$, substitute corresponding sequence-admittance models described by Equations (12)–(15) into the equivalent sequence-admittance in Equation (21), we can derive the equivalent positive-sequence admittance of the traditional GCI, denoted as $Y_{L_ep}(s)$. The relationships of $Y_{L_ep}(s)$ and $Y_{gp}(s)$ at different L_g are presented in Figure 5, where I_1 is 15A and the other parameters are kept consistent with that in Table 1. It can be concluded that the GCI can run stably with $L_g = 14$ mH. While, when L_g is increased to 16 and 18 mH, the phase of $Y_{L_ep}(s)$ at intersection A and B is larger than 90° . As the phase of $Y_{gp}(s)$ is -90° , the phase difference between $Y_{L_ep}(s)$ and $Y_{gp}(s)$ at the intersections exceeds 180° , which indicates the GCI would be unstable.

If the PLL bandwidth is adjusted, Figure 6 depicts the relationships of $Y_{L_ep}(s)$ and $Y_{gp}(s)$ of the traditional GCI equipped with different PLL bandwidths when $L_g = 20$ mH, where f_{PLL} represents the PLL bandwidth. It can be found that reducing f_{PLL} to 100 Hz, the traditional GCI can run stably even when

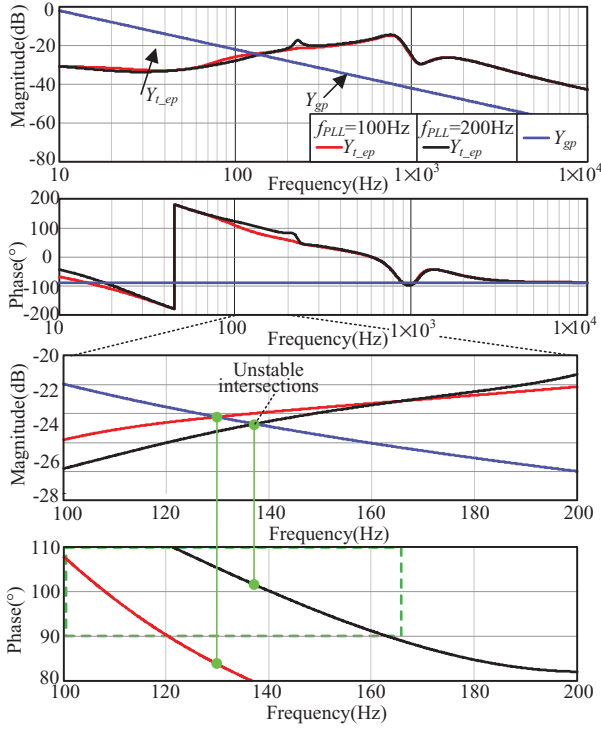


FIGURE 6 Admittances of the grid and the traditional GCI under different f_{PLL} when $L_g = 20\text{mH}$

$L_g = 20\text{mH}$. However, the response speed would be affected if the PLL bandwidth is decreased [3, 4].

4.2 | Stability analysis of the modified GCI only with $K_q = I_1/V_1$

When $K_q = I_1/V_1$ and $K_g = 0$, substitute corresponding sequence-admittance models described by Equations (12), (13), (14) and (15) into Equation (21), we can derive the equivalent positive-sequence admittance of the modified GCI only with the q -axis voltage feedforward control, denoted as $Y_{q-ep}(s)$. The relationships of $Y_{q-ep}(s)$ and $Y_{gp}(s)$ at different L_g are presented in Figure 7, where I_1 is 15A and other parameters are the same as that in Table 1.

From Figure 7, it can be noted that new negative damping regions in middle-frequency range are generated besides the low-frequency ones, and the resonant points are located at the new negative damping regions. That is because of the stronger couplings between $Y_{\phi}(s)$ and $J_{\phi}(s)$ of the modified GCI with $K_q = I_1/V_1$ as depicted in Figure 2. Additionally, it can be seen that the increased grid inductance not only enlarges the newly triggered negative damping region, but also shifts the negative damping region towards a lower frequency range. In Figure 7, the modified GCI with the designed q -axis voltage feedforward only run stably if L_g is 8 mH, with the short circuit ratio (SCR) calculated to be 8.3; when L_g is increased to 10mH, the GCI would resonate at about 220 and 320 Hz; the resonance occurs at lower frequencies with the larger L_g . Therefore, compared

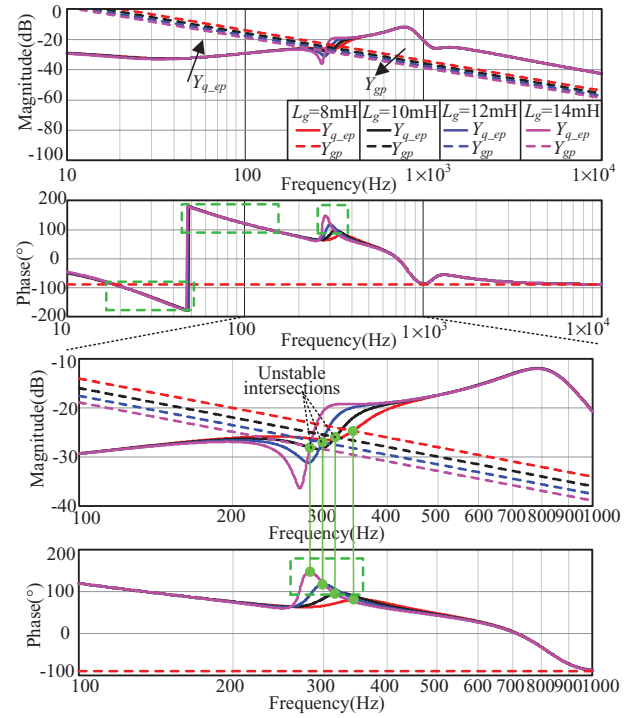


FIGURE 7 Admittances of the grid and the modified GCI with $K_q = I_1/V_1$ under different L_g

with the stability results in Figure 5, the stability of the modified GCI with $K_q = I_1/V_1$ is worse and needs to be further improved to adapt to the weaker grid.

4.3 | Stability analysis of the modified GCI with the proposed coordinated control

Substitute sequence-admittance models described by Equations (12), (13), (14) and (15) into Equation (21), we can derive the equivalent positive-sequence admittance of the modified GCI with the proposed coordinated control, denoted as $Y_{c-ep}(s)$. As shown in Figure 8, if I_1 is 15A and f_{PLL} is 400 Hz, the relationships of $Y_{c-ep}(s)$ and $Y_{gp}(s)$ at different L_g are presented. Other parameters are kept consistent with that in Table 1. It can be observed that the GCI with the developed coordinated control is still stable when L_g grows to 25 mH. While, as shown in Figure 7, the GCI with the designed q -axis voltage feedforward is not stable when L_g is 10 mH. It demonstrates that the stability is greatly improved with the developed PCC-voltage feedforward. Additionally, compare the stability results with that of the traditional GCI, it demonstrates that the GCI with the coordinated control is more applicable to the weak grid.

Furthermore, it should be pointed out that only when K_q is exactly equal to be I_1/V_1 , influences of the PLL bandwidth on stability would be offset. It is easy for the K_q to be adjusted following the variation of the active current I_1 . While, the V_1 term in the K_q is designed to be constant. Therefore, further analysis is carried out to recognize the stability of GCIs with the proposed coordinated control when the grid voltage fluctuates.

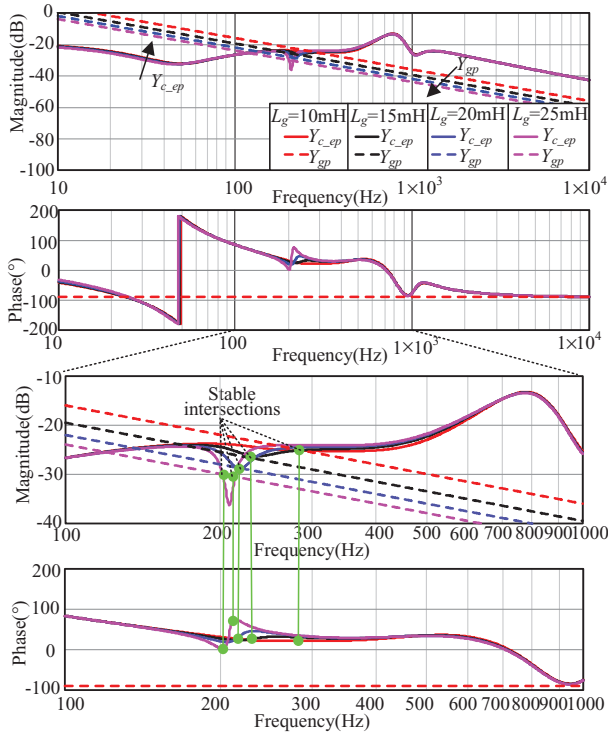


FIGURE 8 Admittances of the grid and the modified GCI with the proposed coordinated control under different L_g

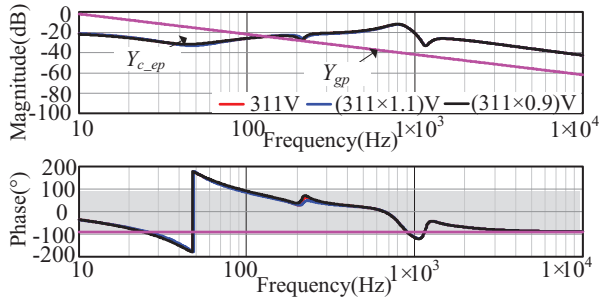


FIGURE 9 Admittances of the grid and the modified GCI with the proposed coordinated control when the grid voltage has fluctuations

Figure 9 depicts the relationships of $Y_{c-ep}(s)$ and $Y_{gp}(s)$ with $L_g = 20$ mH and $f_{PLL} = 300$ Hz. Additionally, V_1 is chosen to be 311 V, (311×1.1) V and (311×0.9) V, respectively, other parameters are the same as that of GCIs in Figure 8. It can be seen that there is sufficient damping at intersections of $Y_{c-ep}(s)$ and $Y_{gp}(s)$ under different V_1 , so the modified GCI with the proposed coordinated control still exhibits good stability in weak grid when the grid voltage has fluctuations.

5 | SIMULATION VERIFICATION

5.1 | Software-only simulation results

By means of the *Plecs* software, Figure 10 shows the simulation results of the traditional GCI with no extra feedforward

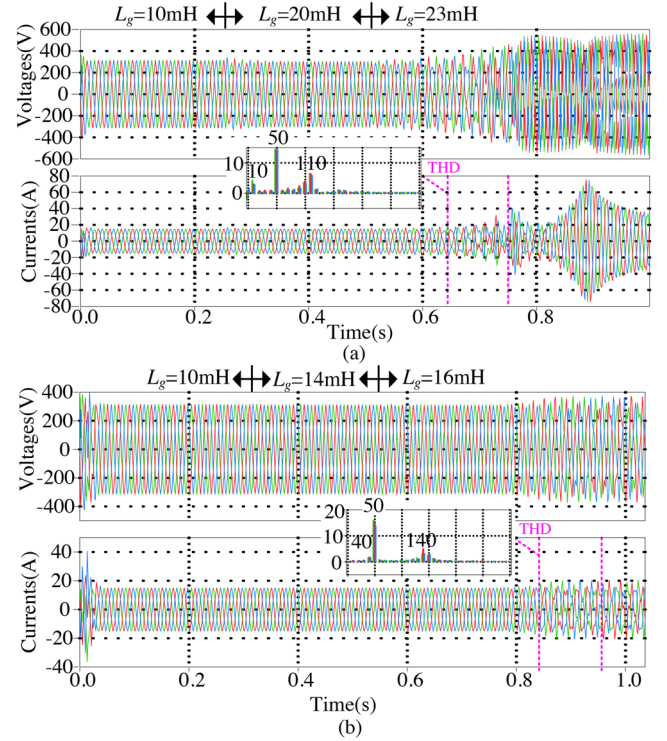


FIGURE 10 Time-domain waveforms of the traditional GCI under different PLL bandwidths (a) $f_{PLL} = 100$ Hz, (b) $f_{PLL} = 200$ Hz

improvement method, where I_1 is 15 A, and the PLL bandwidth f_{PLL} is chosen to be 100 and 200 Hz, respectively. It can be seen from Figure 10 when $f_{PLL} = 100$ Hz, the traditional GCI loses its stability when L_g is increased to 23 mH; while when $f_{PLL} = 200$ Hz, the GCI oscillates with L_g increased to 16 mH. It could be concluded that the weak grid would limit the PLL bandwidth of the traditional GCI, which verifies the stability analyses in Figures 5 and 6.

Figure 11 shows the time-domain simulation results of the modified GCI only with $K_q = I_1/V_1$ under different PLL bandwidths. The GCI is running with $I_1 = 15$ A. It can be drawn that the GCI with $K_q = I_1/V_1$ becomes unstable when L_g is increased to 10 mH despite the PLL bandwidth, which verifies that the stability of the GCI with the designed q -axis voltage feedforward is insensitive to the bandwidth of the PLL. Additionally, as shown in Figure 11d, the resonant frequencies are 200 and 300 Hz, the simulation results validate the stability analysis in Figure 7. Additionally, resonant frequencies in Figure 11 are much larger than those in Figure 10, which verifies the newly generated middle-frequency negative damping because of the designed q -axis voltage feedforward control.

Figure 12 shows the grid-connected voltages and currents of the modified GCI with the proposed coordinated control under varied grid inductance L_g . The GCI is running with $I_1 = 15$ A, and $f_{PLL} = 400$ Hz. It can be found that the proposed coordinated control has a great contribution to ensure the stability of the GCI in weak grids. With the designed parameters, the GCI with the proposed coordinated control starts oscillating at 110 and 210 Hz until L_g is increased to 26 mH.

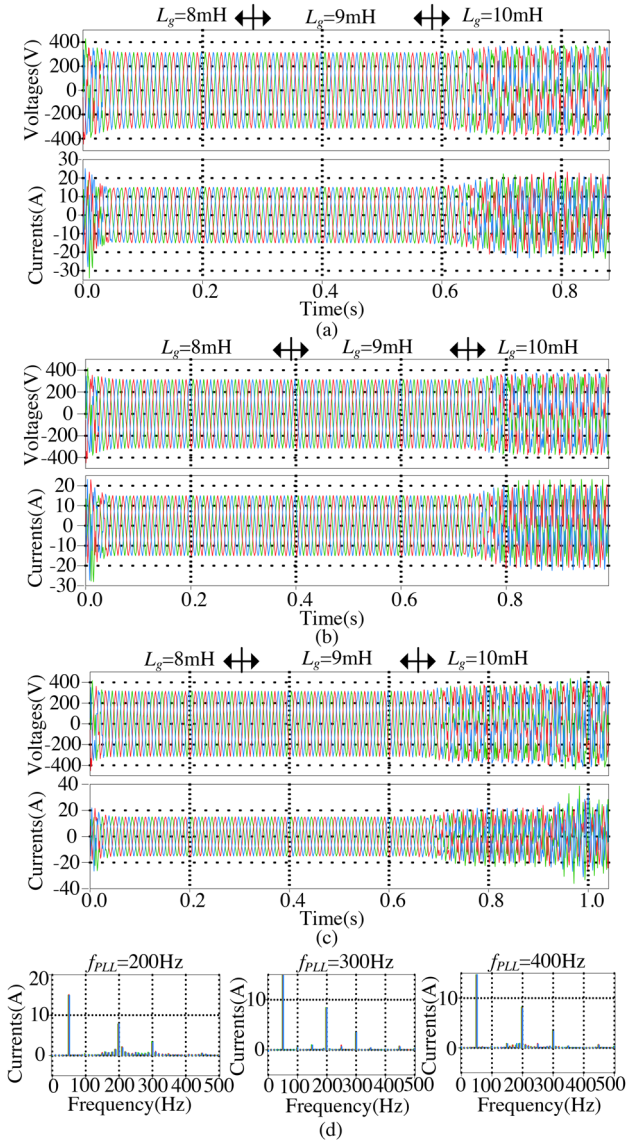


FIGURE 11 Time-domain waveforms of the modified GCI with $K_q = I_1/V_1$ under different PLL bandwidths. (a) $f_{PLL} = 200$ Hz, (b) $f_{PLL} = 300$ Hz, (c) $f_{PLL} = 400$ Hz, (d) THD analysis of the currents when $L_g = 10$ mH

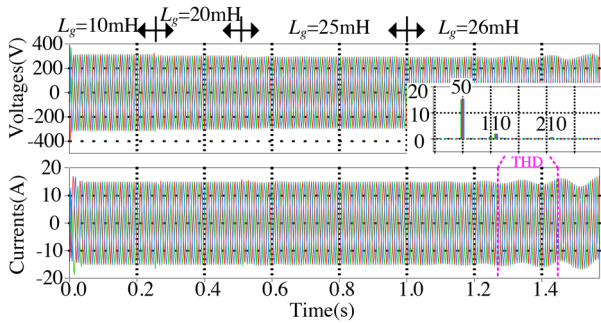


FIGURE 12 Time-domain waveforms of the GCI with the proposed coordinated control under different L_g

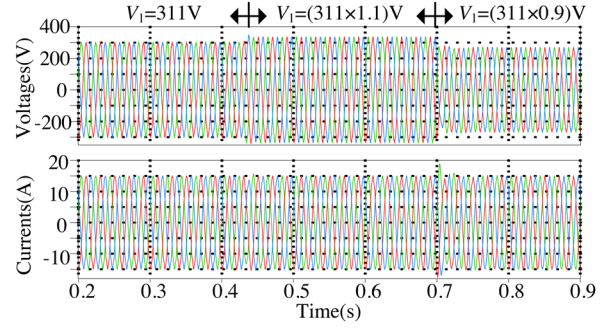


FIGURE 13 Time-domain waveforms of the modified GCI with the proposed coordinated control under different V_1

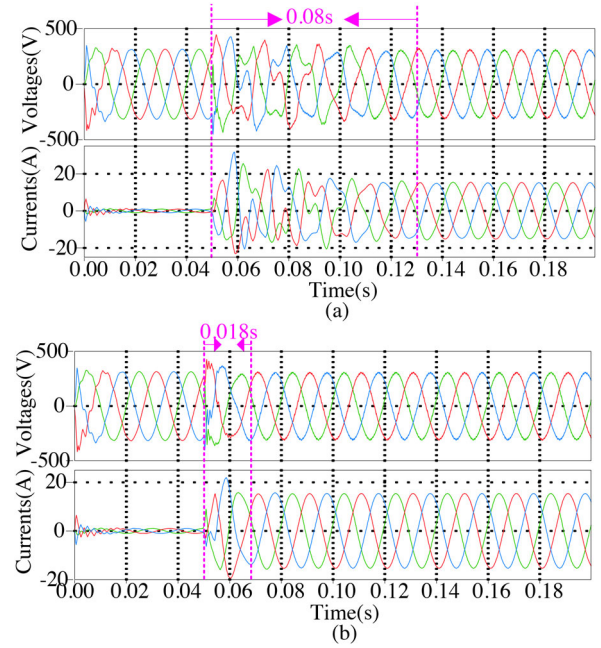


FIGURE 14 Time-domain waveforms of: (a) The traditional GCI, (b) the modified GCI with the proposed coordinated control

Furthermore, when $L_g = 20$ mH and $f_{PLL} = 300$ Hz, Figure 13 shows the grid-connected voltages and currents of the modified GCI with the proposed coordinated control under varied V_1 , which keep sinusoidal when the grid voltage has fluctuations.

Summarily, the modified GCI with the proposed coordinated control can run more stably and shows more robustness in weak grids, which is consistent with the sequence-admittance-based stability analyses in Figures 8 and 9.

Additionally, in order to compare the dynamic response of the GCIs, $L_g = 14$ mH, $I_1 = 15$ A, $K_{pr} = 15$, and $K_{rr} = 15,000$ are selected. Figure 14 shows the step response, where the PLL bandwidth of the traditional GCI is chosen to be 200 Hz to ensure its stable operation under $L_g = 14$ mH. While, for the modified GCI with the proposed coordinated control, the PLL bandwidth has no stability limitations. Here, the PLL bandwidth is chosen to be 400 Hz for the sake of the grid harmonics attenuation. When the switch signal is sent to the GCI at 0.05 s, it

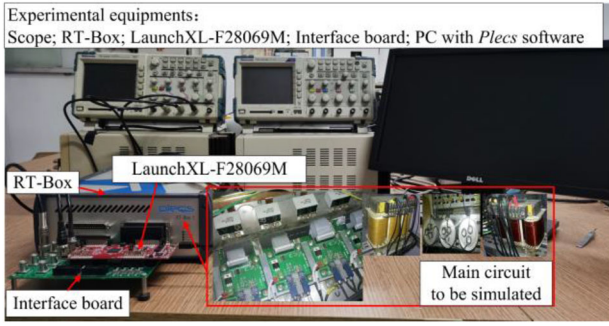


FIGURE 15 HIL platform

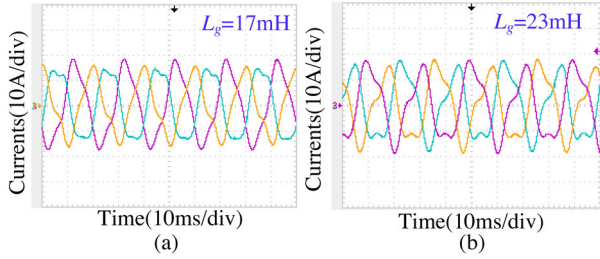


FIGURE 16 HIL simulation results of the traditional GCI under different PLL bandwidths. (a) $f_{PLL} = 200$ Hz, (b) $f_{PLL} = 100$ Hz

can be observed from Figure 14a that for the case of the traditional GCI, it takes 0.08 s to reach the steady-state condition. While, as shown in Figure 14b, the modified GCI with the developed coordinated control can converge to the steady-state within 0.018 s. Therefore, the good dynamical performance of the GCI with the proposed coordinated control is proved by simulations.

5.2 | Hardware-in-the-loop simulation results

As shown in Figure 15, the platform based on hardware-in-the-loop (HIL) is applied to validate the effectiveness of the developed coordinated control with the real DSP chip, where the main circuit depicted in Figure 1 runs in the RT-Box (the deadband and time delay are simulated according to the real main circuit hardware as circled in Figure 15) and the control scheme is realized by the TMS320F28069. The maximum power of the GCI is 10 kW. The sampling period of the main circuit is 10 μ s; the sampling frequency of the control loop is the same as the switching frequency, which is 10 kHz. Other parameters are consistent with those in Table 1. Corresponding waveforms are obtained by a scope (TPS 2024) and the THD analysis is acquired only from the current in Phase A by the power quality analyser (Fluke 435).

Firstly, a test is carried out for the case of the traditional GCI, which is running with 15 A. Other parameters could be found in Table 1. Figure 16 shows the relationships of the PLL bandwidth f_{PLL} and grid inductance L_g . As the grid inductance L_g cannot be changed during the test, L_g is increased by 1 mH at a time. The HIL simulation results show that when the f_{PLL} is

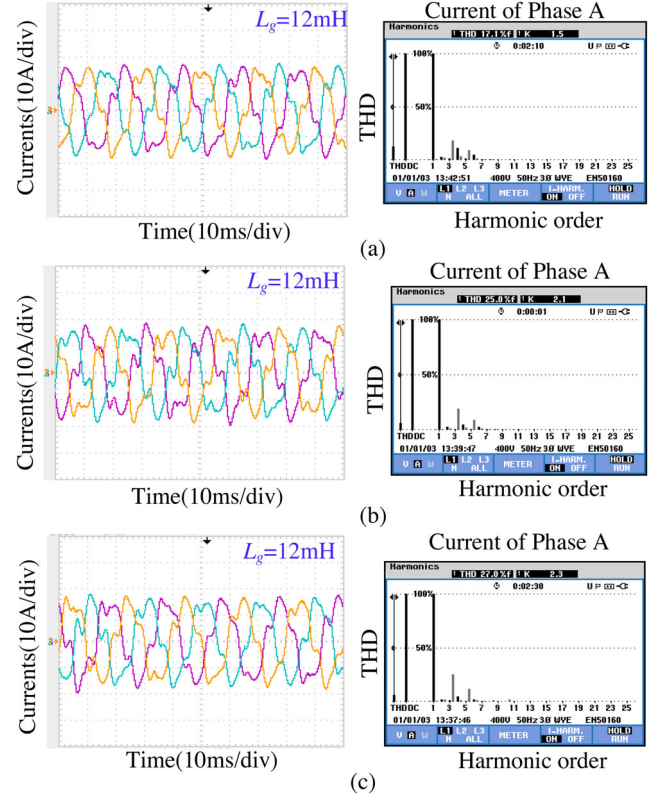


FIGURE 17 HIL simulation results of the modified GCI with $K_q = I_1/V_1$ under different PLL bandwidths. (a) $f_{PLL} = 200$ Hz, (b) $f_{PLL} = 300$ Hz, (c) $f_{PLL} = 400$ Hz

200 Hz, the instability occurs with $L_g = 17$ mH; when the f_{PLL} is decreased to 100 Hz, the instability occurs with $L_g = 23$ mH. The HIL simulation results also verify the stability analysis in Figures 5 and 6.

In theory, the stability of the GCIs with $K_q = I_1/V_1$ is designed to remove the influence of PLL control parameters on the interactive stability. To verify this, the GCIs with $K_q = I_1/V_1$ under test are designed with different PLL control bandwidths, which are $f_{PLL} = 200$ Hz, $f_{PLL} = 300$ Hz, $f_{PLL} = 400$ Hz, respectively. Corresponding HIL simulation results are shown in Figure 17, where $I_1 = 15$ A. It can be seen when L_g is increased to 12 mH, the GCI begins to oscillate at about 150 and 250 Hz no matter what value the PLL bandwidth is set. That verifies the stability of the GCI with $K_q = I_1/V_1$ is irrespective of the PLL controller parameters. It should be noted that there are some differences in the resonant grid inductance compared with Figure 11, which is owing to the different delay between the software-only simulation and HIL platform. The difference would not influence the stability conclusions in this paper.

When the developed PCC-voltage feedforward is introduced to the modified GCI with $K_q = I_1/V_1$, corresponding HIL simulation results are depicted in Figure 18. Figure 18a shows the waveforms of the GCI with the control scheme changes from the proposed coordinated control to the designed q -axis feedforward control when $L_g = 20$ mH. The grid-connected currents change from the stable mode to unstable mode, which confirms the effectiveness of the added PCC-voltage

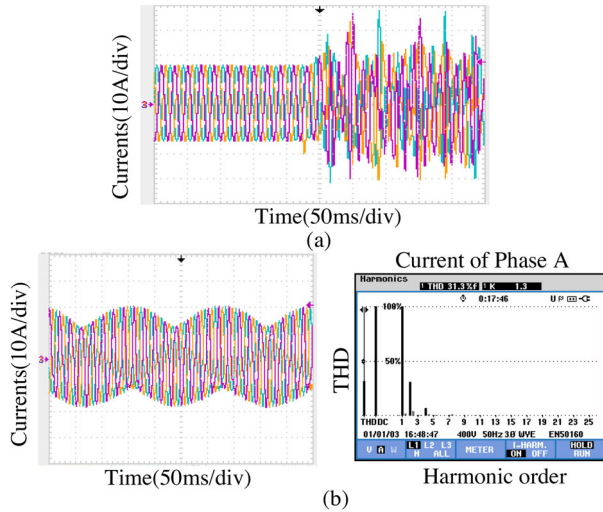


FIGURE 18 HIL simulation results of the modified GCI with: (a) Control scheme changes from the proposed coordinated control to the only q -axis voltage control when $L_g = 20$ mH, (b) the proposed coordinated control when $L_g = 25$ mH

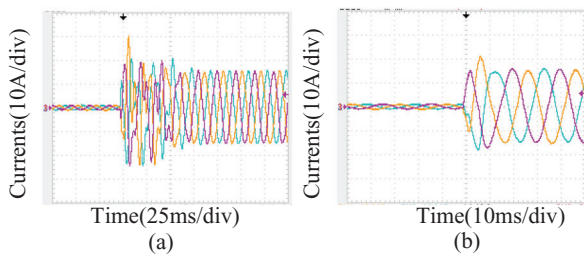


FIGURE 19 HIL simulation results of: (a) The traditional GCI, (b) the modified GCI with the proposed coordinated control

feedforward. Furthermore, by increasing the L_g , the GCI with the proposed coordinated control becomes unstable when L_g rises to 25 mH ($SCR = 2.6$). The resonant currents are shown in Figure 18b, whose resonant frequencies are about 100 and 200 Hz. Compared with Figure 16, it is clear that the modified GCI with the developed coordinated control is more robust to the weak grids.

To test the dynamic response, Figure 19 collects the waveforms of the GCI with and without the developed coordinated control when $L_g = 14$ mH. The PLL bandwidth of the traditional GCI is set to be 200 Hz to ensure the stability. As shown in Figure 19, it takes the traditional GCI about 75 ms to reach the steady-state, while, it only takes the GCI with the developed coordinated control about 10 ms to converge to the steady-state. The HIL simulation results also verify that the dynamic response speed of the GCI is greatly enhanced by the proposed coordinated control.

6 | CONCLUSIONS

For the weak-grid-connected GCI, an important concern is about the interactive stability issues resulting from the PLL.

Commonly, the dynamic response and the stability relating to the PLL are difficult to balance. To tackle the contradictions, this paper proposes a coordinated control that is composed of the designed q -axis voltage feedforward and the developed PCC-voltage feedforward. Specifically, the designed q -axis voltage feedforward reshapes the sequence-admittances of the GCI and the dynamics of the PLL are removed from the modified admittances. Therefore, the stability of the modified GCI is verified to have no interaction with the bandwidth of the PLL and the PLL controller parameters can be regulated without the limitation from the stability concerns. However, the modified admittances show worse phase characteristics and corresponding negative damping is deteriorated. Then the PCC-voltage feedforward is developed to cooperate with the designed q -axis voltage feedforward by phase compensation, thus gain stability and dynamic performance improvement of GCIs in weak grids.

Although the pure q -axis voltage feedforward, the pure PCC-voltage feedforward or PLL-removal control schemes have been previously proposed to improve the PLL-related stability, feedforward coefficients of the designed coordinated control in this paper are much simpler to be applied and the PLL dynamics can be eliminated without changing the widely used current control scheme. Additionally, the designed feedforward coefficients are not connected with the GCI control and grid impedance.

FUNDING

National Natural Science Foundation of China (62073095), Science & Technology Projects from the State Grid Heilongjiang Electric Power Co., Ltd (522437200038).

CONFLICT OF INTEREST

All authors have no conflict of interest to disclose.

PERMISSION TO REPRODUCE MATERIALS FROM OTHER SOURCES

None.

DATA AVAILABILITY STATEMENT

Data available on request from the authors.

ORCID

Xuemei Zheng  <https://orcid.org/0000-0002-3037-1334>

REFERENCES

- Golestan, S., Monfared, M., Freijedo, F.D.: Design-oriented study of advanced synchronous reference frame phase-locked loops. *IEEE Trans. Power Electron.* 28(2), 765–778 (2013)
- Dong, D., Wen, B., Boroyevich, D., et al.: Analysis of phase-locked loop low-frequency stability in three-phase grid-connected power converters considering impedance interactions. *IEEE Trans. Ind. Electron.* 62(1), 310–321 (2015)
- Zhou, S., Zou, X., Zhu, D., et al.: An improved design of current controller for LCL-type grid-connected converter to reduce negative effect of PLL in weak grid. *IEEE J. Emerg. Sel. Topics Power Electron.* 6(2), 648–663 (2018)
- Zhu, D., Zhou, S., Zou, X., Kang, Y.: Improved design of PLL controller for LCL-type grid-connected converter in weak grid. *IEEE Trans. Power Electron.* 35(5), 4715–4727 (2020)

5. Wang, X., Blaabjerg, F.: Harmonic stability in power electronic based power systems: Concept, modeling, and analysis. *IEEE Trans. Smart Grid.* 10(3), 2858–2870 (2019)
6. Li, C.: Unstable operation of photovoltaic inverter from field experiences. *IEEE Trans. Power Del.* 33(2), 1013–1015 (2018)
7. Sun, J.: Impedance-based stability criterion for grid-connected inverters. *IEEE Trans. Power Electron.* 26(11), 3075–3078 (2011)
8. Wen, B., Boroyevich, D., Burgos, R., et al.: Analysis of D-Q small-signal impedance of grid-tied inverters. *IEEE Trans. Power Electron.* 31(1), 675–687 (2016)
9. Fang, J., Li, X., Li, H., Tang, Y.: Stability improvement for three-phase grid-connected converters through impedance reshaping in quadrature-axis. *IEEE Trans. Power Electron.* 33(10), 8365–8375 (2018)
10. Shuai, Z., Li, Y., Wu, W., et al.: Divided DQ small-signal model: A new perspective for the stability analysis of three-phase grid-tied inverters. *IEEE Trans. Ind. Electron.* 66(8), 6493–6504 (2019)
11. Cespedes, M.: Impedance modeling, analysis, and adaptation of grid connected inverters with PLL. Ph.D. dissertation, Rensselaer Polytechnic Institute, Troy, NY (2014)
12. Bakhshizadeh, M.K., Wang, X., Blaabjerg, F., et al.: Coupling in Phase Domain Impedance Modelling of Grid-Connected Converters. *IEEE Trans. Power Electron.* 31(10), 6792–6796 (2016)
13. Zhang, C., Cai, X., Rygg, A., Molinas, M.: Sequence domain SISO equivalent models of a grid-tied voltage source converter system for small-signal stability analysis. *IEEE Trans. on Energy Convers.* 33(2), 741–749 (2018)
14. Nian, H., Chen, L., Xu, Y., Huang, H., Ma, J.: Sequences domain impedance modeling of three-phase grid-connected converter using harmonic transfer matrices. *IEEE Trans. on Energy Convers.* 33(2), 627–638 (2018)
15. Li, G., Wang, W., Liu, C., et al.: Mechanism analysis and suppression method of wideband oscillation of pmsg wind farms connected to weak grid (part I): Analysis of wideband impedance characteristics and oscillation mechanism. *Proc. CSEE* 39(22), 6547–6661 (2019)
16. Li, G., Wang, W., Liu, C., et al.: Mechanism analysis and suppression method of wideband oscillation of PMSG wind farms connected to weak grid (part II): Suppression method of wideband oscillation based on impedance reshaping. *Proc. CSEE* 39(23), 6908–6920 (2019)
17. Zhang, X., Xia, D., Fu, Z., et al.: An improved feedforward control method considering PLL dynamics to improve weak grid stability of grid-connected inverters. *IEEE Trans. Ind. Appl.* 54(5), 5143–5151 (2018)
18. Chen, X., Zhang, Y., Wang, S., et al.: Impedance-phased dynamic control method for grid-connected inverters in a weak grid. *IEEE Trans. Power Electron.* 32(1), 274–283 (2017)
19. Yang, D., Wang, X., Liu, F., et al.: Symmetrical PLL for SISO impedance modeling and enhanced stability in weak grids. *IEEE Trans. Power Electron.* 35(2), 1473–1483 (2020)
20. Zhang, X., Fu, S., Chen, W., et al.: A symmetrical control method for grid-connected converters to suppress the frequency coupling under weak grid conditions. *IEEE Trans. Power Electron.* 35(12), 13488–13499 (2020)
21. Gui, Y., Wang, X., Wu, H., Blaabjerg, F.: Voltage-modulated direct power control for a weak grid-connected voltage source inverters. *IEEE Trans. Power Electron.* 34(11), 11383–11395 (2019)
22. Yu, Y., Ma, H., Zheng, X., et al.: Coupling-related instability mechanism and mitigation analysis of the instantaneous power based current controlled inverter. *IEEE Access* 8, 178909–178923 (2020)

How to cite this article: Yu, Y., Zheng, X., Li, H., Guerrero, J.M., Akhavan, A.: Coordinated control to achieve stability and dynamic response enhancement of weak-grid-connected inverters based on sequence-admittance models. *IET Renew. Power Gener.* 16, 339–351 (2022)

<https://doi.org/10.1049/rpg2.12327>